Atmospheric Environment 125 (2016) 152–164

Contents lists available at ScienceDirect

Atmospheric Environment

journal homepage: www.elsevier.com/locate/atmosenv

Mixing state of atmospheric particles over the North China Plain

S.L. Zhang[a,c,d], N. Ma[d,*], S. Kecorius[d], P.C. Wang[a], M. Hu[b], Z.B. Wang[d,e], J. Größ[d], Z.J. Wu[b], A. Wiedensohler[d]

[a] Key Laboratory of Middle Atmosphere and Global Environment Observation, Institute of Atmospheric Physics, Chinese Academy of Sciences, Beijing, 100029, China
[b] College of Environmental Sciences and Engineering, Peking University, Beijing, 100871, China
[c] Chengdu University of Information Technology, Chengdu, 610225, China
[d] Leibniz Institute for Tropospheric Research, Leipzig, 04318, Germany
[e] Multiphase Chemistry Department, Max Planck Institute for Chemistry, Mainz, 55128, Germany

HIGHLIGHTS

- A HTDMA and a VTDMA were used together in a unique field study in China.
- A certain fraction of hydrophobic particles is volatile.
- Minor difference was found between the mixing states for different air mass types.
- Submicron particles in North China Plain are external mixture of two major groups.

ARTICLE INFO

Article history:
Received 17 June 2015
Received in revised form 4 October 2015
Accepted 19 October 2015
Available online 21 October 2015

Keywords:
Mixing state
Hygroscopicity
Volatility
Aerosol particles
North China Plain

ABSTRACT

In this unique processing study, the mixing state of ambient submicron aerosol particles in terms of hygroscopicity and volatility was investigated with a Hygroscopicity Tandem Differential Mobility Analyzer and a Volatility Tandem Differential Mobility Analyzer. The measurements were conducted at a regional atmospheric observational site in the North China Plain (NCP) from 8 July to 9 August, 2013. Multimodal patterns were observed in the probability density functions of the hygroscopicity parameter κ and the shrink factor, indicating that ambient particles are mostly an external mixture of particles with different hygroscopicity and volatility. Linear relationships were found between the number fraction of hydrophobic and non-volatile populations, reflecting the dominance of soot in hydrophobic and non-volatile particles. The number fraction of non-volatile particles is lower than that of hydrophobic particles in most cases, indicating that a certain fraction of hydrophobic particles is volatile. Distinct diurnal patterns were found for the number fraction of the hydrophobic and non-volatile particles, with a higher level at nighttime and a lower level during the daytime. The result of air mass classification shows that aerosol particles in air masses coming from north with high moving speed have a high number fraction of hydrophobic/non-volatile population, and are more externally mixed. Only minor differences can be found between the measured aerosol properties for the rest of the air masses. With abundant precursor in the NCP, no matter where the air mass originates, as far as it stays in the NCP for a certain time, aerosol particles may get aged and mixed with newly emitted particles in a short time.

1. Introduction

The mixing state of atmospheric particles is a key feature for understanding their role in the atmosphere (Jacobson et al., 2000; Riemer et al., 2009; Oshima et al., 2009). It determines climate-relevant aerosol physical properties such as cloud condensation nuclei activity (Furutani et al., 2008; Zelenyuk et al., 2010; Wu et al., 2013b), hygroscopicity (Johnson et al., 2005; Herich et al., 2009; Liu et al., 2011) and optical properties (Jacobson, 2001; Moffet and Prather, 2009; Zaveri et al., 2010). Moreover, information on the aerosol mixing state is also necessary for accurate assessment of environmental problems (Laborde et al., 2013; Healy et al., 2014; Kamilli et al., 2014) and health effects (Schnelle-Kreis et al., 2009;

* Corresponding author.
E-mail address: ma@tropos.de (N. Ma).

http://dx.doi.org/10.1016/j.atmosenv.2015.10.053

Londahl et al., 2010; Yang et al., 2014), and reducing uncertainties in global and regional aerosol models (Cappa et al., 2012; Reddington et al., 2013; Riemer et al., 2009).

The use of tandem differential mobility analyzers (TDMA) has been proven to be an effective way to determine particle mixing state and give indirect insights on chemical composition of particles (Swietlicki et al., 2008). A Volatility Tandem Differential Mobility Analyzer (VTDMA) in conjunction with a Differential Mobility Particle Sizer (DMPS) was used to determine the number and mass concentration of externally mixed less-volatile particles in urban background air (Frey et al., 2008). It was shown that the mass concentration of less-volatile particles agrees well with measured black carbon mass concentration. Wehner (Wehner et al., 2009), Rose (Rose et al., 2011) and Cheng (Cheng et al., 2012) estimated the mixing state of soot particle based on the fraction of low-volatile group from VTDMA measurements at Yufa, China in Aug. – Sep. 2006. Wehner (Wehner et al., 2009) indicated that the fraction of externally mixed soot particles decreased from about 37% during clean periods to 18% during heavily polluted periods. Tiitta (Tiitta et al., 2010) used a VTDMA system together with hygroscopic and organic TDMAs to study the composition of ultrafine particles near the major roads in Kuopio, Finland. In a laboratory study by Hossain (Hossain et al., 2012), VTDMA system was used to investigate the mixing state of size-selected ultrafine aerosol particles emitted from different biomass burning sources. The mixing state of aerosol particles from rice straw, oak and pine burning under different conditions including smoldering combustion, flaming combustion and open burning were analyzed. The VTDMA was also successfully applied in combustion engine exhaust studies in dynamometers by Burtscher (Burtscher et al., 2001).

Massling (Massling et al., 2009) and Liu (Liu et al., 2011) carried out aerosol hygroscopicity experiments applying a Hygroscopicity Tandem Differential Mobility Analyzer (HTDMA) in Beijing (Jun. – Jul. 2004, Jan. – Feb. 2005) and Wuqing (Jul. – Aug. 2009), respectively. Massling (Massling et al., 2009) reported the number fraction of freshly emitted soot to be 20–32% depending on dry particle sizes and seasons. Liu (Liu et al., 2011) found that the aerosol mixing state varied significantly during the day, and the number fraction of externally mixed hydrophobic particles was about 8% during daytime and 20% at night. Possible correlations between non-voylatile particles and hydrophobic particles were analyzed by Kuwata (Kuwata et al., 2007; Kuwata and Kondo, 2008) and Rose (Rose et al., 2011). Kuwata (Kuwata et al., 2007) showed that most of less hygroscopic particles were less volatile, while more hygroscopic particles were likely to be more volatile. Similar conclusion was found by Rose during a campaign near Guangzhou, China (Rose et al., 2011).

The North China Plain (NCP), including a group of megacities (Beijing and Tianjin), is an area with great industrial activity and dense population, consuming large amounts of fossil fuels like coal, gasoline, diesel and natural gas (Liu et al., 2009; Zong et al., 2015). As a consequence, large amounts of particulate and gaseous pollutants are emitted into the atmosphere causing severe air pollution (Tao et al., 2012; Liu et al., 2015). The widespread combustion of fossil fuels and biomass makes the NCP a significant source of light absorbing carbonaceous aerosol (LAC), which plays an important role in the global radiative balance (Cheng et al., 2009; Wehner et al., 2009). With high particle loading and abundant precursor in the NCP, the mixing state of aerosol particles might be complex, and its influence on aerosol climatic and environmental effects might also be specific. Recent assessments of aerosol radiative effects (Zhuang et al., 2013; Nordmann et al., 2014) have highlighted the importance of particle mixing state in reducing the uncertainties in climate models and in improving pollution control strategies. By applying parallel measurements of V- and HTDMA system in the NCP, we aim to have a better understanding of the impact of different aerosol sources and transformation processes on the particle mixing state in polluted areas. Tiitta (Tiitta et al., 2010) has demonstrated the advantages of using different TDMAs in parallel to investigate the properties of aerosol particles. V- and HTDMA system setup gives not only information on inorganic contribution but also on the temperature-dependent aerosol component which separates the contribution of black carbon. To our knowledge, such a setup was applied for the first time in the NCP.

In this study, an overview of the parallel measurements of VTDMA and HTDMA is presented. Then a comparison between the number fraction of non-volatile particles and hydrophobic particles was done. Diurnal variations of particle mixing state, as well as volatility and hygroscopicity were discussed. Air mass back trajectory analysis was carried out to investigate the impact of different aerosol sources and transportation processes on particle mixing state. At last, we parameterized the measured size-dependent particle mixing state to facilitate further applications.

2. Experiment

2.1. Measurement site

During the field campaign (8 July to 9 August, 2013), aerosol microphysical and optical properties were measured at Xianghe station (39.75 °N, 116.96 °E, 36 m a.s.l.), a regional site in the NCP about 70 km southeast from Beijing. The measurement site is located at the outskirts of a small village about 5 km west to the Xianghe town center. The surroundings are residential areas and farm land. Fig. 1 shows the average aerosol optical depth (AOD) distribution during summer from 2012 to 2014 over the NCP, monitored by the Ozone Monitoring Instrument (OMI) with a high

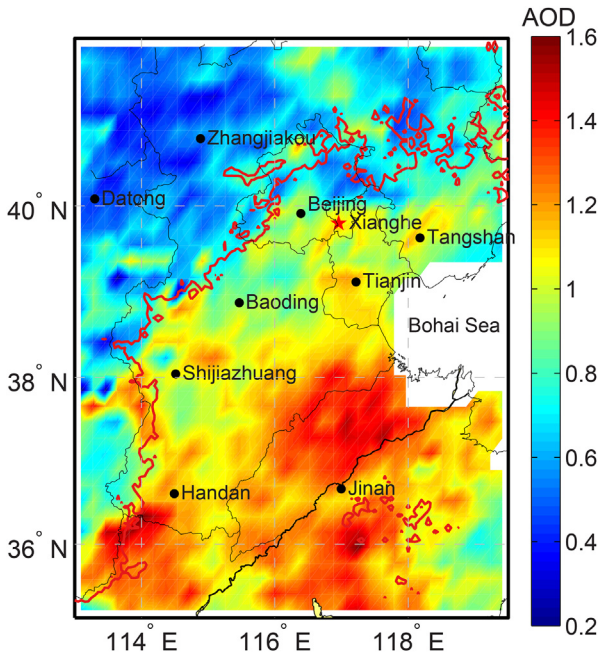

Fig. 1. Map of the North China Plain. The measurement site is marked with red star. Black dots show the major cities in the NCP. Contour plot shows the 3-year summer average OMI AOD distribution (2012–2014, 0.25° × 0.25° resolution). The red solid line denotes the 500 m contour line of elevation height, which can be considered as the boundary of the NCP.

spatial resolution of 0.25° × 0.25° at 483.5 nm (Livingston et al., 2009) which shows a reasonable agreement with MODIS and MISR observations over most of the major emission sources (Ahn et al., 2008). As shown in Fig. 1, high level of AOD can be found in the whole NCP, and Xianghe station is located near the north boundary of this region.

During the campaign period, the predominant wind directions were from the southwest and southeast. The average relative humidity (RH), temperature (T), and wind speed (WS) were 96.6%, 23.2 °C (min: 19.6 °C, max 27.6 °C), and 0.4 m/s for nighttime (18:00–09:00 Local Time); and were 75.2%, 27.5 °C (min 20.5 °C, max: 36.5 °C), and 1 m/s for daytime (09:00–18:00 LT), respectively.

2.2. Instruments

Most of the measurements were conducted in a temperature-controlled (24 °C) measurement container built by Leibniz-Institute for Tropospheric Research (TROPOS). Atmospheric aerosol was sampled by an inlet system consisting of a PM10 inlet (Rupprecht & Patashnick Co., Inc., Thermo, 16.67 L/min), followed by a 1.5 m Nafion dryer (Wiedensohler et al., 2013) and an automatic drying chamber (Tuch et al., 2009). This setup ensured an aerosol sample with RH always below 30%. In the measurement container, sampled air was fed to separate instruments through an isokinetic flow splitter and stainless steel/conductive tubing (Wiedensohler et al., 2013). Two Tandem Differential Mobility Analyzers (TDMA) based systems (HTDMA and VTDMA; Leibniz-Institute for Tropospheric Research, Germany), accompanied with a mobility particle size spectrometer type TROPOS-SMPS (Scanning Mobility Particle Sizer; Leibniz-Institute for Tropospheric Research, Germany; Wiedensohler et al., 2012), an Multi-Angle Absorption Photometer (MAAP Model 5012; Thermo, Inc., Waltham, MA USA) and a integrating nephelometer (Model 3563; TSI, Inc., Shoreview, MN USA) were used to measure size-resolved particle hygroscopicity and volatility, particle number size distribution (PNSD), LAC mass concentration, and particle scattering coefficient, respectively.

2.2.1. HTDMA

During the field campaign, particle hygroscopic growth factor (*GF*), defined as $GF(RH) = D(RH)/D_d$, was measured with a HTDMA (Massling et al., 2003) at RH of 87% and initial dry particle diameters (D_d) of 50, 100, 150, 200, 250 and 350 nm. One full scan for all the six sizes took about 50 min. The TDMA*inv* developed by Gysel et al. (2009) was used for data inversion.

The measurement uncertainty of the HTDMA mainly depends on the accuracy of RH in the second differential mobility analyzer (DMA) and the possible size shift between the two DMAs (Massling et al., 2007). To correct the RH measured by the dew point mirror, the growth factor of ammonium sulfate particles of 100 nm dry diameter at 87% RH were measured periodically (each 6 h). The estimated uncertainty in RH was ±1% RH, resulting in a relative uncertainty of around 2.5% for *GF*s of ammonium sulfate particles at 90% RH (Massling et al., 2003). Since ammonium sulfate particles are unable to take up water at RH lower than the deliquescence point (about 80%), the size shift between the two DMAs for the entire data set was corrected using the dry scans (without humidifying). Polystyrene Latex Spheres (PSL, Thermo Scientific, Duke Standards) of 203 nm were used to calibrate the offset in sizing by the two DMAs. PSL sizing checks were performed on regular bases (once per week) during the whole measurement campaign. The offset in sizing was observed to be less than 3%, which agrees well with the recommendations for such systems (Wiedensohler et al., 2012).

2.2.2. VTDMA

Particle volatility was determined by a VTDMA (Philippin et al., 2004). The VTDMA has a similar structure as the HTDMA with the only difference in the conditioning unit – the humidifier is replaced with a volatilization column, where volatile compounds would evaporate at 300 °C revealing non-volatile particles or cores (Burtscher et al., 2001). Species, which do not evaporate at 300 °C are referred to as non-volatile compounds in this study. PNSD of residual were obtained from the electrical mobility spectra measured by the second DMA and condensation particle counter (CPC), taking into account charging probabilities (Wiedensohler, 1988), counting efficiency of the condensation particle counter (Wiedensohler et al., 2007), transfer function (Birmili et al., 2007), diffusion and thermophoresis losses. The residence time of the particles in the heating column was 0.5 s, which is sufficient to evaporate the volatile fraction of particles in a narrow size range (Philippin et al., 2004). The same dry particle diameters as HTDMA measurement (50, 100, 150, 200, 250, 300 and 350 nm) was selected for VTDMA measurement. The temporal resolution of full scans was about 50 min. The TDMA*inv* developed by Gysel (Gysel et al., 2009) was used for the data inversion. Ambient temperature (25 °C) scans were used to correct the size shift between the two DMAs and define the width of the transfer function (Gysel et al., 2009). 203 nm PSL particles were used to calibrate the offset in sizing of the two DMAs on weekly basis. In general, the uncertainty in sizing and number counting is ±3% and ±10%, respectively (Philippin et al., 2004).

2.2.3. Additional instrumentation and measurements

The mobility particle size spectrometer, which was used to measure PNSD, consists of a Hauke-type medium-DMA (28 cm effective length) and a CPC (Model 3772; TSI, Inc., Shoreview, MN USA) (Wiedensohler et al., 2012). It can measure PNSD with a size range from 10 to 850 nm.

The LAC mass concentration was measured with a MAAP (Model 5012; Thermo, Inc., Waltham, MA USA) with a temporal resolution of 1 min at a wavelength of 637 nm. The aerosol absorption coefficient (σ_{ap}) can be calculated with a mass absorption cross section of 6.6 $m^2\ g^{-1}$ (Petzold and Schonlinner, 2004). To be able to measure at highly polluted conditions in the NCP, the flow was adjusted to 3 l/min by installing a custom made nozzle.

Particle scattering coefficient (σ_{sp}) was measured with a nephelometer (Model 3563; TSI, Inc., Shoreview, MN USA) at 450, 550 and 700 nm with same temporal resolution as MAAP. The truncation and non-Lambertian error was corrected using a modified Mie model (Ma et al., 2011). The single scattering albedo (SSA), defined as $SSA = \sigma_{sp}/(\sigma_{sp} + \sigma_{ap})$, is one of the most important parameters in estimating of the direct aerosol radiative forcing. To calculate SSA at a wavelength of 637 nm, a wavelength correction is applied to the measured σ_{sp} using an empirical approach, $\sigma_{sp} \propto \lambda^{\alpha}$. The Ångström exponent (α) is yielded from the measured σ_{sp} at a wavelength of 550 nm and 700 nm.

2.3. Methodology

2.3.1. Hygroscopicity parameter and its probability density function

To facilitate the comparison of the measured particle hygroscopicity at different RHs, the hygroscopicity parameter κ is calculated (Petters and Kreidenweis, 2007):

$$\kappa(GF) = \left(GF^3 - 1\right) \cdot \left[\frac{1}{S} \exp\left(\frac{4\sigma_{s/a} M_W}{RT\rho_W D_d GF}\right) - 1\right] \quad (1)$$

where S represents the saturation ratio; ρ_W is the density of water; M_W is the molecular weight of water; $\sigma_{s/a}$ is the surface tension of

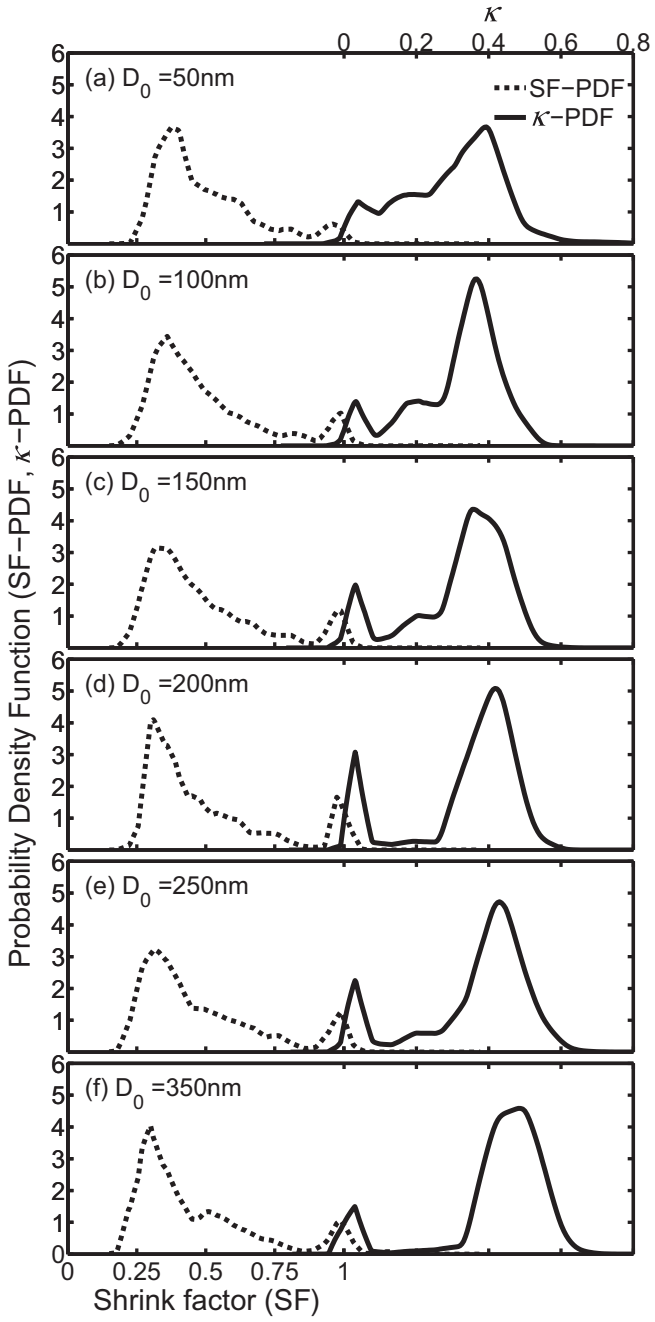

Fig. 2. Averaged probability density functions of hygroscopicity parameter κ (κ-PDF, solid lines) and shrink factor (SF-PDF, dashed lines).

the solution/air interface which is assumed to be the same as the surface tension of the pure water/air interface; R is the universal gas constant; T is the temperature.

Moreover, to investigate the mixing state of aerosol species with different hygroscopicity, the Probability Density Function of GF (GF-PDF, $c(GF,D_d)$) and κ (κ-PDF, $c(\kappa,D_d)$) are introduced as follows,

$$\int_0^\infty c(GF, D_d) \cdot dGF = 1 \tag{2}$$

$$\int_0^\infty c(\kappa, D_d) \cdot \mathrm{d}\kappa = 1 \tag{3}$$

2.3.2. Shrink factor and its probability density function

Shrink factor (SF) is defined as a ratio between the diameter of particles at 300 °C ($D(T)$) and the dry diameter at ambient temperature (D_d):

$$SF = \frac{D(T)}{D_d} \tag{4}$$

Similarly, the Probability Density Function of SF (SF-PDF, $c(SF, D_d)$) is calculated as:

$$\int_0^\infty c(SF, D_d) \cdot dSF = 1 \tag{5}$$

The volume fraction (VF) of non-volatile particles and compounds (at 300 °C) is calculated from the following equation:

$$\mathrm{VF}_{NV} = \int_0^\infty SF \cdot c(SF, D_d) \cdot dSF \tag{6}$$

Thorough information about VTDMA data evaluation can be found in Cheng et al. (2009) and Wehner et al. (2009).

2.3.3. Number fraction, the mean hygroscopicity and shrink factor

Due to the complex mixing state of ambient aerosol particles, different groups in terms of hygroscopicity and volatility of particles were frequently observed in several field campaigns over the NCP. Based on previous studies (Wehner et al., 2009; Liu et al., 2011) and our measurement results (shown in Fig. 2), ambient aerosol particles were classified into three groups in terms of hygroscopicity (hydrophobic group, slight-hydrophilic (SH) group, and very-hydrophilic (VH) group) and three groups in terms of volatility (non-volatile group (NV), slight-volatile (SV) group, and very-volatile (VV) group). The κ and SF are used here to define the boundaries for each group:

Hydrophobic population: $\kappa < 0.1$;
Slight-hydrophilic (SH) population: $0.1 \leq \kappa < 0.25$;
Very-hydrophilic (VH) population: $\kappa \geq 0.25$;
Non-volatile (NV) population: SF ≥ 0.88;
Slight-volatile (SV) population: $0.5 \leq$ SF < 0.88;
Very-volatile (VV) population: SF < 0.5.

The number fraction (NF), average κ (κ_{mean}) and SF (SF_{mean}) for each group with a boundary of [a,b] is defined as:

$$\mathrm{NF} = \begin{cases} \int_a^b c(\kappa, D_d) \cdot d\kappa, & \text{for HTDMA scans} \\ \int_a^b c(SF, D_d) \cdot dSF, & \text{for VTDMA scans} \end{cases} \tag{7}$$

$$\kappa_{mean} = \int_a^b \kappa \cdot c(\kappa, D_d) \cdot d\kappa \tag{8}$$

$$\mathrm{SF}_{mean} = \int_a^b SF \cdot c(SF, D_d) \cdot dSF \tag{9}$$

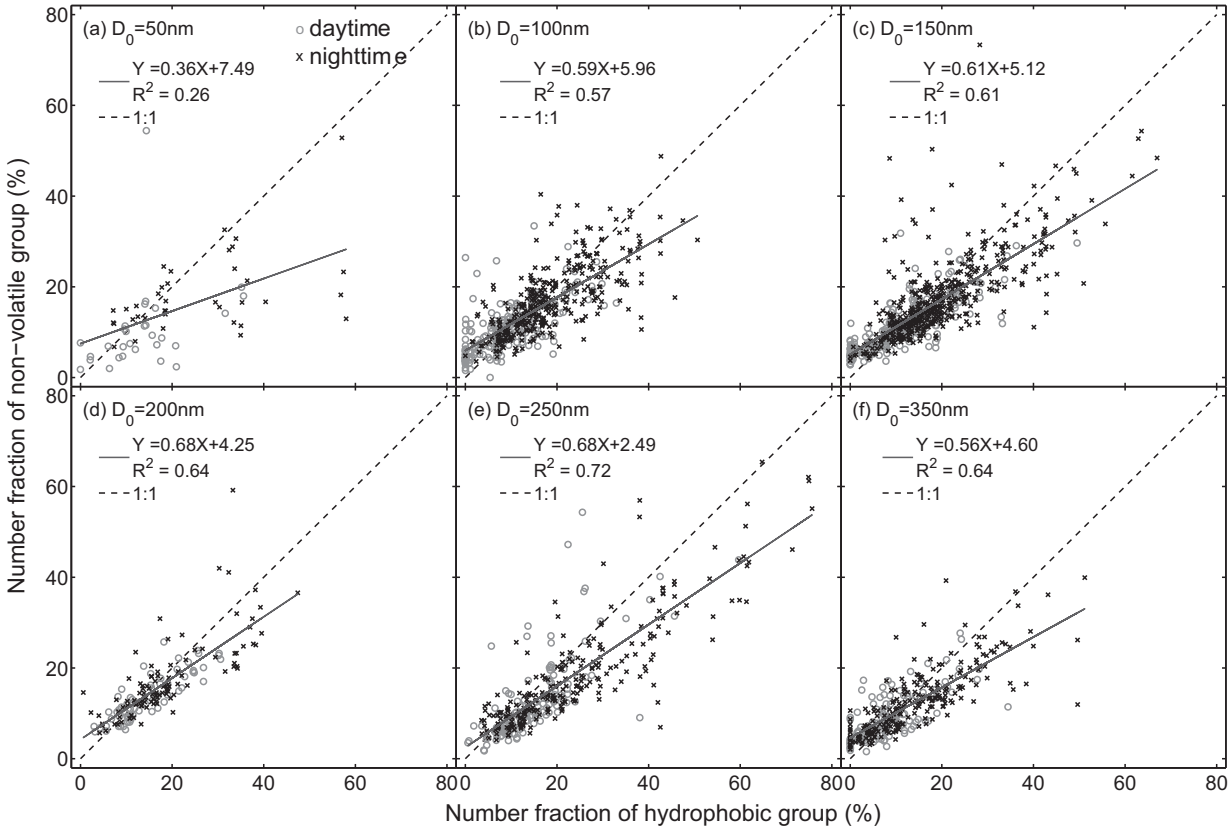

Fig. 3. Comparison between the number fractions of hydrophobic group and non-volatile group.

2.3.4. Air mass classification

Regional atmospheric particle properties are related to the history of the air masses. Back trajectories are therefore useful to trace the history of air masses and to get a better insight into relevant processes during transportation (Wehner et al., 2008). The air mass back trajectory analysis was carried out using a PC version Hybrid Single Particle Lagrangian Integrated Trajectory (HYSPLIT) model and Global Data Assimilation System (GDAS) analysis set. The HYSPLIT model is developed by NOAA Air Resource Lab (ARL) (Draxler and Hess, 1997, 1998; Draxler, 1999). The GDAS analysis set provides meteorological fields every 6 h with a spatial horizontal resolution of 1° × 1° and a vertical resolution corresponding to standard pressure levels (1000, 925, 850 hPa, etc.). Back trajectories arriving 72 h back in time were calculated at a starting level of 500 m above the ground.

3. Results and discussions

3.1. Overview of the measurement

During the whole campaign period from 8 Jul. to 9 Aug., the initial particle sizes set for the HTDMA and the VTDMA were 50 nm, 100 nm, 150 nm, 200 nm, 250 nm and 350 nm. The numbers of valid scans were 720, 1300, 1293, 385, 756 and 1095 for HTDMA, and 823, 688, 862, 180, 685 and 422 for VTDMA for the six sizes, respectively.

Fig. 2 shows the average κ-PDF (solid lines) and SF-PDF (dashed lines) for the 6 measured sizes. Generally, multimodal patterns were observed for κ-PDF, including a dominant very-hydrophilic mode and a smaller but distinct hydrophobic mode. The very-hydrophilic mode peaks at κ from about 0.32 to 0.46 for particles from 50 to 350 nm. The hydrophobic mode does not exhibit significant shifting with the particle size changing. The SF-PDFs also exhibit multimodal behaviors, with a dominant very-volatile mode and a smaller, but distinct non-volatile mode. The very-volatile modes peak at SF from about 0.38 to 0.3, and shift towards smaller SF with the size increasing. Similar with hydrophobic mode, the non-volatile mode does not show evident shifting with different particle sizes. It should be noted that a third mode can be found in κ-PDF for particles smaller than 150 nm. Such a tri-modal pattern of κ-PDF was also observed in other studies (Kecorius et al., 2015; Tan et al., 2013; Zhang et al., 2011; Kulmala et al., 2001). Moreover, it is clear that the classification of three different groups (described in Sect. 2.3.3) for particles is appropriate, because the hydrophobic mode and very-hydrophilic mode for most scans at all sizes are adequately captured.

The distribution of SF-PDF and κ-PDF demonstrates the mixing state of particles/compounds in terms of volatility and hygroscopicity in ambient aerosol particles. The multimodal patterns in SF-PDF and κ-PDF indicate that ambient particles are mostly in an external mixture of two major groups.

As introduced in Sect. 2.1, there are some residential areas nearby our station, thus the measurement might be influenced by local anthropogenic emissions, especially during the nighttime. As shown in Fig. 4b, particle total volume concentration shows a clear peak at 20:00 LT and remains at a high level during the whole night, resulting from high local emission (traffic, cooking) and weak vertical mixing in the nighttime. Particle hygroscopicity and volatility also show a feature of fresh emitted anthropogenic particles (details will be discussed in Section 3.3). Therefore, for a better regional representation, statistics of the measurements are based on only daytime data (09:00–18:00 LT). Actually, the influence of local anthropogenic emissions on our measurements might always

exist. However, the traffic rush hours and the cooking time, during which the local emission has strong influence, are excluded from the daytime period defined here. And the developing of boundary layer in daytime causes a vertical mixing, thus might weaken the influence of local emission. Therefore, the influence of local anthropogenic emission is relatively small. And the measurements in daytime are assumed to be representative of the region.

Statistics of HTDMA and VTDMA measurements in daytime are summarized in Table 1. In general, the ensemble mean particle hygroscopicity increases with particle sizes, and is slightly higher than that observed at another station in the NCP in 2009 (Liu et al., 2011). The volume fraction of non-volatile compounds is around 0.23 for all the measured sizes.

3.2. Relationship between non-volatile and hydrophobic particles

Non-volatile components at 300–350 °C in submicron particles can be assumed to be representative of LAC particles in the NCP (Wehner et al., 2009; Frey et al., 2008; Rose et al., 2006). LAC is also one of the major hydrophobic components in particulate matter (Jacobson et al., 2000; Riemer et al., 2010). Therefore, the non-volatile group in SF-PDF and hydrophobic group in κ-PDF is supposed to be correlated to the externally mixed LAC particles. To better understand the relationship between non-volatile particles and hydrophobic particles, the measured number fraction of non-volatile group (NF_{NV}) is compared with the measured number fraction of hydrophobic group (NF_{phb}). Nighttime data (marked as 'x' in black) and daytime data (marked as 'o' in gray) of NF_{NV} and NF_{phb} are shown in Fig. 3.

Generally, weak linear relationships can be found between NF_{phb} and NF_{NV}, especially for particles larger than 100 nm. The determination coefficients (R^2) are respectively 0.57, 0.61, 0.64, 0.72 and 0.64 for diameter of 100, 150, 200, 250 and 350 nm, respectively (See Fig. 3b–f). All the slopes of linear fits are lower than 1, indicating that a certain fraction of hydrophobic particles are volatile. Similar measurement in Tokyo found that 10–17% of hydrophobic particles are completely volatile (Kuwata et al., 2007). Primary particles from lubricant oil emitted from motor vehicles might be one possible species of this hydrophobic but volatile particles (Sakurai et al., 2003). It should be noted that the slope of linear fit is only 0.36 for 50 nm, indicating that only a minor fraction of hydrophobic particles are non-volatile. This is because primary LAC particles are mainly in the size range larger than 50 nm (Harris and Maricq, 2001), the major composition of 50 nm hydrophobic particles is probably volatile insoluble organic matter.

The linear correlations between NF_{phb} and NF_{NV} shown in Fig. 3 indicate that those two groups are very likely to be dominated by the same component, i.e. LAC. However, the R^2 is not really high since the data points are widely scattered. This might be attributable to two reasons. Firstly, completely volatile particles such as externally mixed organics and ammonium sulfate, are usually not taken into consideration in the mixing state in terms of volatility, since they are not visible in the SF-PDF measured by VTDMA. The number fraction of non-volatile particles thus might be overestimated. The degree of the overestimation depends on the number fraction of completely volatile particles which might vary with time, and cause the dispersing of the data points in Fig. 3. Secondly, as mentioned above, some insoluble particles are volatile at 300 °C, resulting in a number fraction of hydrophobic group greater than the number fraction of non-volatile group. Since the number fraction of insoluble non-volatile particles may vary largely with time, the relationship of the two number fractions does not follow a strict linear correlation.

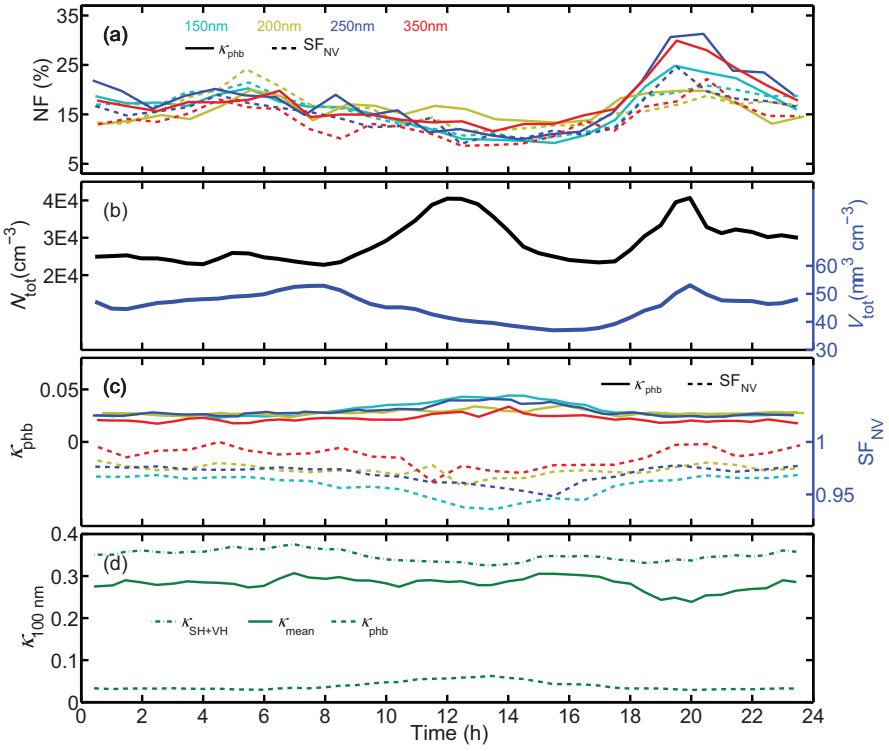

Fig. 4. Diurnal variations of (a) number fraction of hydrophobic particles and non-volatile particles, (b) total particle number and volume concentrations, (c) average κ of hydrophobic particles and SF non-volatile particles, and (d) avergage κ of different groups for 100 nm particles. Different color represent different initial dry diameters in subplot (a) and (c).

Table 1
Summary of the HTDMA and VTDMA measurements during the Xianghe campaign. Statistics are based on only daytime (09:00–18:00 LT) data.

Dry diameter (nm)	50	100	150	200	250	350
Hydrophobic population (κ < 0.1)						
Mean GF ± STD	1.087 ± 0.034	1.069 ± 0.028	1.071 ± 0.031	1.06 ± 0.017	1.067 ± 0.025	1.04 ± 0.03
Mean κ±STD	0.056 ± 0.023	0.039 ± 0.017	0.038 ± 0.018	0.031 ± 0.009	0.034 ± 0.014	0.02 ± 0.015
Mean NF ± STD	0.123 ± 0.122	0.101 ± 0.082	0.116 ± 0.082	0.152 ± 0.072	0.125 ± 0.101	0.138 ± 0.122
Slight-hydrophilic population (SH, 0.1 < κ < 0.25)						
Mean GF ± STD	1.283 ± 0.036	1.279 ± 0.032	1.285 ± 0.042	1.277 ± 0.054	1.275 ± 0.051	1.282 ± 0.055
Mean κ±STD	0.211 ± 0.033	0.185 ± 0.025	0.183 ± 0.032	0.174 ± 0.041	0.17 ± 0.038	0.173 ± 0.041
Mean NF ± STD	0.274 ± 0.273	0.165 ± 0.188	0.102 ± 0.129	0.029 ± 0.03	0.06 ± 0.092	0.026 ± 0.048
Very-hydrophilic population (VH, κ > 0.25)						
Mean GF ± STD	1.449 ± 0.05	1.472 ± 0.036	1.498 ± 0.038	1.535 ± 0.028	1.544 ± 0.047	1.581 ± 0.046
Mean κ±STD	0.378 ± 0.057	0.365 ± 0.038	0.38 ± 0.04	0.412 ± 0.03	0.42 ± 0.051	0.455 ± 0.051
Mean NF ± STD	0.603 ± 0.318	0.734 ± 0.219	0.782 ± 0.174	0.819 ± 0.084	0.815 ± 0.174	0.836 ± 0.153
Ensemble mean of all populations from HTDMA						
Mean GF ± STD	1.364 ± 0.09	1.405 ± 0.067	1.43 ± 0.066	1.454 ± 0.043	1.473 ± 0.089	1.501 ± 0.096
Mean κ±STD	0.291 ± 0.089	0.299 ± 0.064	0.312 ± 0.063	0.329 ± 0.043	0.348 ± 0.084	0.373 ± 0.092
Non-volatile population (NV, SF > 0.88)						
Mean SF ± STD	0.921 ± 0.029	0.936 ± 0.026	0.947 ± 0.023	0.97 ± 0.016	0.961 ± 0.025	0.977 ± 0.032
Mean NF ± STD	0.12 ± 0.075	0.11 ± 0.058	0.118 ± 0.057	0.134 ± 0.052	0.115 ± 0.084	0.111 ± 0.072
Slight-volatile population (SV, 0.5 < SF < 0.88)						
Mean SF ± STD	0.572 ± 0.046	0.57 ± 0.027	0.578 ± 0.022	0.583 ± 0.019	0.584 ± 0.022	0.58 ± 0.026
Mean NF ± STD	0.441 ± 0.207	0.349 ± 0.134	0.327 ± 0.131	0.301 ± 0.087	0.302 ± 0.144	0.285 ± 0.122
Very-volatile population (VV, SF < 0.5)						
Mean SF ± STD	0.366 ± 0.028	0.356 ± 0.033	0.347 ± 0.034	0.345 ± 0.023	0.332 ± 0.039	0.323 ± 0.032
Mean NF ± STD	0.463 ± 0.255	0.538 ± 0.154	0.555 ± 0.154	0.565 ± 0.115	0.583 ± 0.191	0.604 ± 0.147
Ensemble mean volume fraction of non-volatile compounds from VTDMA						
Mean VF ± STD	0.247 ± 0.097	0.233 ± 0.09	0.234 ± 0.094	0.235 ± 0.077	0.228 ± 0.125	0.21 ± 0.118

3.3. Diurnal variation

To investigate the diurnal variations of the mixing state, hygroscopicity and volatility of aerosol particles, the average diurnal variations of κ, *SF*, number fractions of hydrophobic mode and non-volatile mode, as well as the total number and volume concentrations (N_{tot}, V_{tot}) during the whole campaign are present in Fig. 4.

Distinct diurnal patterns of NF_{phb} can be seen in Fig. 4a, with a higher level during nighttime and a lower level during daytime. NF_{NV} shows a similar diurnal pattern but with less amplitude compared with NF_{phb}. Both NF_{phb} and NF_{NV} show a daily maximum at around 20:00 LT. In the evening, large amount of primary particles with low hygroscopicity and volatility (mainly LAC) are emitted from traffic sources and accumulate in the nocturnal boundary layer, which also can be seen as a peak in the diurnal variation of V_{tot} (Fig. 4b). Emission from cooking is very likely to contribute on the hydrophobic and non-volatile fractions (Zhang et al., 2014). Accidental open burning might also be a contributor. With deactivated aging processes during nighttime, those particles remain externally mixed (Petters et al., 2006; Zhang et al., 2008), and cause high level of NF_{phb} and NF_{NV} during the whole nighttime. A small peak can be seen for both NF_{phb} and NF_{NV} at around 06:00 LT. This is because human activity has started at this time but secondary particle production might be still weak. During the daytime between 09:00 and 18:00 LT, local anthropogenic emission is lower, and the active aging processes facilitate the mixing of primary particles with secondary species. Also, the developing of boundary layer may entrain the more aged particles from aloft. Therefore, the number fraction of hydrophobic particles and non-volatile particles are at a relatively low level (around 10%). Those externally mixed non-volatile and hydrophobic particles are likely to originate from the traffic emission in daytime in the area. This diurnal variation of particle mixing state agrees with the result derived from particle optical properties in the NCP (Ma et al., 2012).

The average κ of hydrophilic particles (including slight-hydrophilic and very-hydrophilic groups) shows an opposite diurnal variation compared with hydrophobic particles (Fig. 4d). One possible explanation is, some primary hydrophobic particles (mainly LAC) grow up quickly to the size we measured via aging processes in the daytime. Although mixed with secondary particle species, which is to a large extent hydrophilic (e.g. ammonium sulfate), the overall hygroscopicity of these particles is still low due to the existence of LAC. However, those particles are grouped into hydrophilic mode, resulting in a lower average κ in daytime (Wiedensohler et al., 2009). Similar results were also reported in previous studies (Moffet and Prather, 2009; Rose et al., 2011).

In order to see the dependence of particle mixing state on its size, the average diurnal variations of κ-PDF and SF-PDF for all measured sizes during the entire campaign are shown in Fig. 5. Generally, κ-PDF and SF-PDF show inversion symmetrical patterns. Two distinct modes can be seen from the distributions at most of the measured sizes. As discussed above, the very-hydrophilic mode for particles larger than 100 nm shifts towards lower kappa in daytime. A slight shift towards higher SF can be also seen for the very-volatile mode for particles larger than 100 nm, but is not as clear as the shift in very-hydrophilic mode and nearly invisible for 250 and 350 nm. The hydrophobic mode and non-volatile mode is much stronger at nighttime than in daytime. It should be noted that the diurnal variation of κ-PDF and SF-PDF for 50 nm is slightly different from those for larger diameters. For 50 nm particles, the slight-hydrophilic mode moves towards higher κ and the slight-volatile mode moves towards lower SF in the morning, which is very likely to be caused by new particle formation (Wu et al., 2013a). New particle formation events occurred during the whole campaign period, which can be seen in the average diurnal variation of particle total number concentration as a pronounced peak with a decreasing particle total volume concentration in the afternoon (Fig. 4d). It was found that the growth of the newly formed particles is mainly contributed by sulfate and organic matters in Beijing area (Yue et al., 2011; Zhang et al., 2011). During the growth, the increase of the volume fraction of sulfate and oxidized organics in particulate matter results in an increase in κ and decrease in SF of

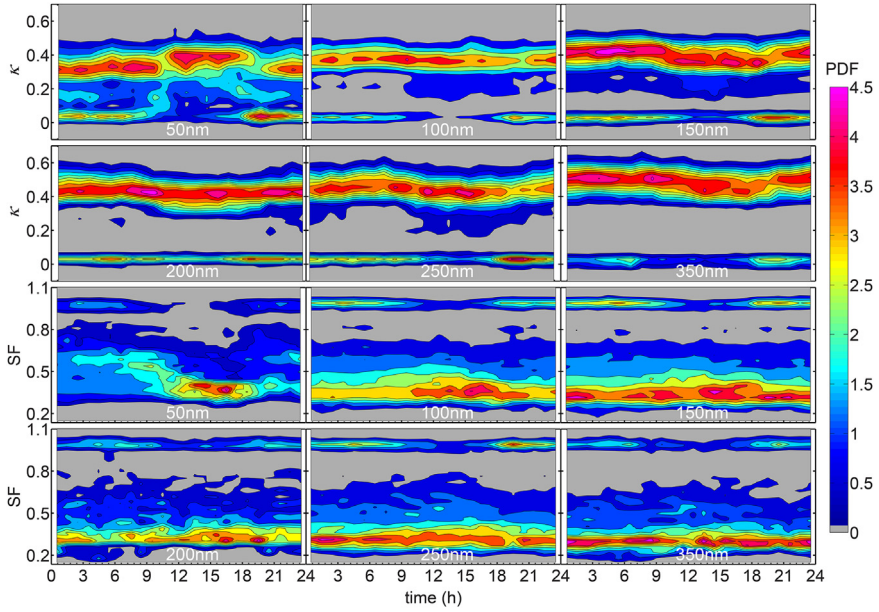

Fig. 5. Diurnal variations of κ-PDF and SF-PDF at six measured particles sizes.

50 nm particles, as shown in Fig. 5. Similar variation of hygroscopicity of ultrafine particles was also found in the former studies in Finland (Kulmala et al., 2001; Ehn et al., 2007), Germany (Wu et al., 2013a), and China (Kecorius et al., 2015).

3.4. Particle hygroscopicity, volatility and mixing state in different air masses

In the NCP, synoptic-scale air masses can be a concept to explain the variations of hygroscopicity, volatility and mixing state of aerosol particles. To investigate the influence of air mass origin and transportation on these aerosol properties, our measurement data was classified according to the types of back trajectory obtained with NOAA HYSPLIT model described in Section 2.3.4.

Seven clusters were carried out based on 144 back trajectories, and the mean trajectory of each cluster is shown in Fig. 6. The air mass moving speed is illustrated with markers on the mean trajectories (the duration of transporting between two markers is 6 h). Xianghe station is mainly influenced by the air masses originated from southwest (Cluster 4) and north (Cluster 3, 5, 2, 1 and 7). Air masses in cluster 2–5, which account for 76% of all trajectories mainly transported with low speed and altitudes. Air masses in the other two clusters (Cluster 1 and 7) move with relatively high speeds. It should be noted that cluster 6 only consist of 3 trajectories which always stays at a height of 200 m. These three trajectories are in the period when East China is under the influence of tropical storm Leepi. Therefore, cluster 6 is excluded in the following discussion due to its weak representativeness (the results under cluster 6 are included in Figs. 7–9).

Air masses in cluster 2–5 stayed within a height lower than 1500 m for more than 30 h. Such a long residence time in the boundary layer over the NCP is enough for particles to be well aged in the air masses (Wehner et al., 2009). Single scattering albedo represents the relative contribution of particle scattering on extinction. During the aging processes, SSA for dry state particles may increase due to the secondary production of particulate matter. SSA therefore can reflect the degree of aging of aerosol particles to some extent. As shown in Fig. 7, high SSA and V_{tot} but low N_{tot} were observed for cluster 2–5, indicating a high degree of aging of aerosol particles. In contrast, the V_{tot} and SSA for air masses in cluster 1 and 7 are at a low level, since these air masses have very short residence time over the NCP so that aerosol particles in the air masses are less aged (Meng et al., 2009).

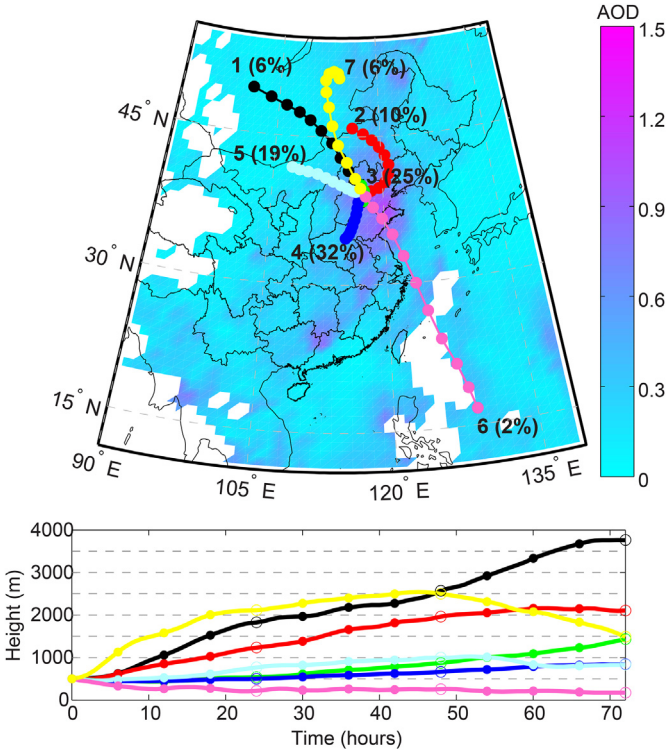

Fig. 6. Average back trajectories of the seven types of air masses over the NCP. Contour plot in the background of the map represen the average AOD.

The average κ, NF_{phb} and NF_{NV} for the seven clusters are shown in Fig. 8. In general, results for cluster 1 and 7 are quite similar, but largely different from those for the rest clusters. The average κ for cluster 1 and 7 is around 0.2 at all the measured sizes, lower

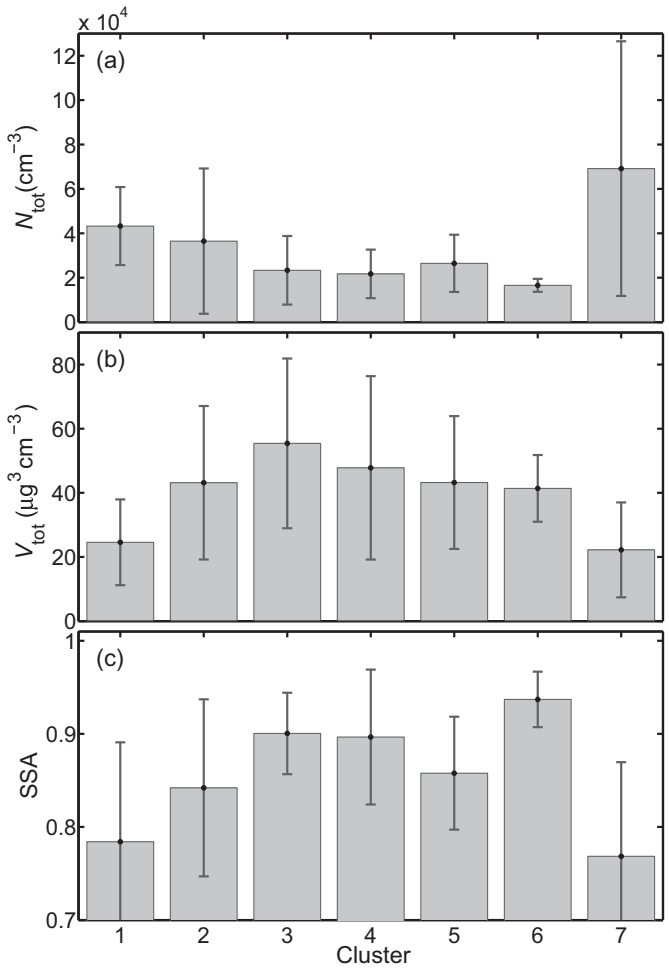

Fig. 7. Single scattering albedo (SSA, λ = 637 nm), particle total number and volume concentrations (N_{tot}, V_{tot}) for the seven types of air masses.

than those for the rest clusters. The average NF_{phb} and NF_{NV} for cluster 1 and 7 is higher than those for cluster 2–5 at most of the measured sizes. As discussed above, air masses of cluster 1 and 7 mainly transport in a high altitude (higher than 1500 m) above the clean area with inactive secondary aerosol production, and then experience a strong downward motion just before arriving at the measurement site. Therefore, aeorosol particles do not have enough time to be well aged. Primary hydrophobic and non-volatile particles remain externally mixed, resulting in high level of NF_{phb} and NF_{NV}.

It should be noted that only minor differences can be found between the results of cluster 2–5. This is probably because of the high activity of the secondary aerosol production in the NCP. With abundant precursors in the NCP (Zhang et al., 2014; Shen et al., 2011; Xu et al., 2011), no matter where the air mass originates, as long as it enters the boundary layer over the NCP, particles may get aged in a short time and mixed with newly emitted particles. Therefore the aerosol particles of cluster 2–5 show similar hygroscopicity independent of their origin. Within cluster 2–5, lower κ_{mean} and higher NF_{phb} can be found for cluster 2 and 5 comparing with the other two clusters, probably because the residence time of the air mass of cluster 2 and 5 in the mixing layer over the NCP is shorter than the other two clusters (see Fig. 6).

To further investigate the influence of aerosol sources and transportation on its mixing state, the average κ-PDF and SF-PDF for the seven clusters are shown in Fig. 9. Generally, the average κ-PDF and SF-PDF show similar pattern for cluster 2–5, which is quite different from the results for cluster 1 and 7. Since particles are more likely to become similar in chemical composition during the aging processes (Tan et al., 2013), only one hydrophilic mode can be found in cluster 2–5. As a contrast, with short residence time over the NCP, aerosol particles in air mass of cluster 1 and 7 are less aged, hence are more diverse in chemical compostion. Two hydrophilic modes, including distinct slight-hydrophilic mode ($0.1 < \kappa < 0.25$ in cluster 1; $0.1 < \kappa < 0.3$ in cluster 7) and a very-hydrophilic mode ($0.25 < \kappa < 0.6$ in cluster 1; $0.3 < \kappa < 0.6$ in cluster 7), appear in the κ-PDF of cluster 1 and 7. For the SF-PDF, multimodal distributions are observed for all the seven clusters. Comparing with cluster 2–5, the volatile mode in cluster 1 and 7 shifts towards higher SFs (shown in Fig. 9b), also because aerosol particles for these two clusters are less aged than cluster 2–5.

3.5. Parameterization of particle hygroscopicity and volatility

Hygroscopicity and volatility parameters of aerosol particles were measured only for several individual diameters in this study. To facilitate the use of this information, the measured parameters were parameterized as functions of dry diameter D_P with:

$$f(D_P) = B \cdot \log(D_P) + C \cdot D_P + D \quad (10)$$

Where, B, C and D are fitting parameters. This equation was used in the parameterization of hygroscopicity parameter κ and number fraction of each group (Rissler et al., 2006; Liu et al., 2011), and was also used for the parameterization of the results from VTDMA.

The average κ and number fraction of very-hydrophilic group and hydrophobic group, as well as the average SF and number fraction of very-volatile group and non-volatile group at measured diameters are shown in Fig. 10. As mentioned in Sect. 3.1, nighttime measurements are sometimes influenced by local anthropogenic emissions. Therefore, only daytime results are parameterized in this section.

For the average κ of very-hydrophilic group particles, the minimum was found at 100 nm. The average κ increases obviously with the increase of dry diameter for the particles larger than 100 nm. The average κ of hydrophobic group decreases with the increase of particle diameter. Similar dependence of κ on particle diameter was also found in another site in the NCP (Liu et al., 2011). The absolute values in Liu et al. (2011) are somehow different from our results, due to different boundaries of groups which were chosen in their study. The relationships between SF for each group and particle diameters are nearly linear. With the increase of particle diameter, the average SF for very-volatile mode decreases slightly, while it increases slightly for non-volatile mode. Representing mainly the externally mixed LAC, both number fractions of non-volatile mode and hydrophobic mode show almost the same values at the size range measured, at about 12%. The number fractions of very-hydrophilic mode and very-volatile mode increase with the increase of particle diameter, with a higher slope for 50–150 nm and a lower slope for 150–350 nm.

The fitting results are shown as dashed lines in Fig. 10. It can be seen that the fitting curves match the measurements quite well. The fitting parameters B, C and D are listed in Table 2. It should be noted that without any measured data points, it is not recommended to use Eq. (10) and the parameters in Table 2 for $D_P > 350$ nm or $D_P < 50$ nm.

4. Conclusion

To investigate the aerosol mixing state in terms of hygroscopicity and volatility in the north NCP, we performed Hygroscopicity

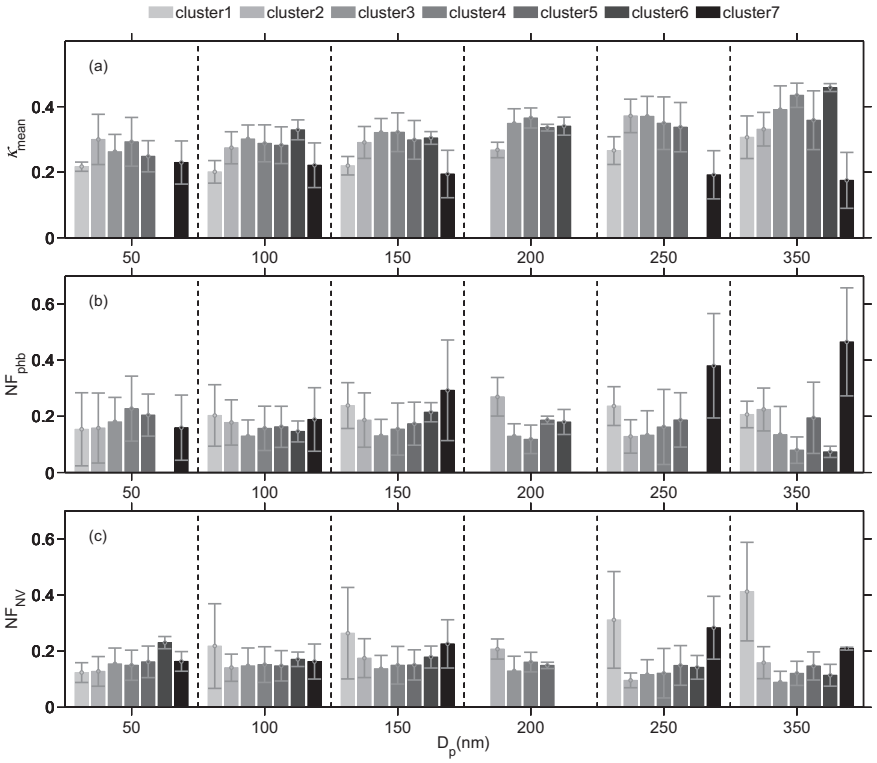

Fig. 8. Average hygroscopicity parameter (κ), and number fraction of hydrophobic population (NF_{phb}) and non-volatile population (NF_{NV}) for the seven air mass types and six measured sizes.

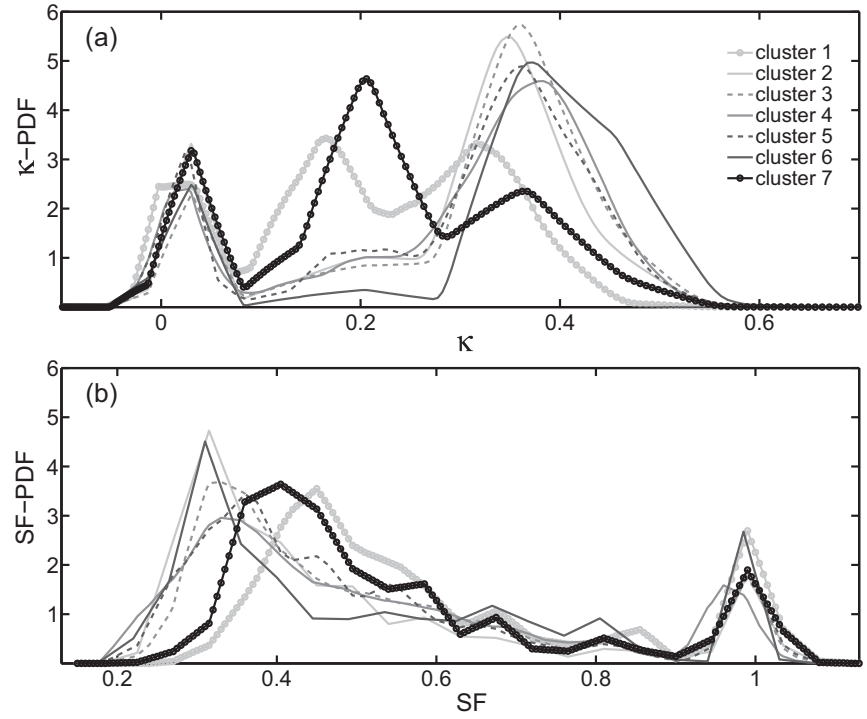

Fig. 9. Average κ-PDF and SF-PDF of 100 nm particles for the seven air mass types.

Tandem Differential Mobility Analyzer and Volatility Tandem Differential Mobility Analyzer measurements at a regional atmospheric observational site in the north NCP in July and August in 2013.

Multimodal patterns were observed in both κ-PDF and SF-PDF, including a dominant very-hydrophilic mode/very-volatile mode and a smaller but distinct hydrophobic mode/non-volatile mode, indicating that ambient particles are mostly in an external mixture

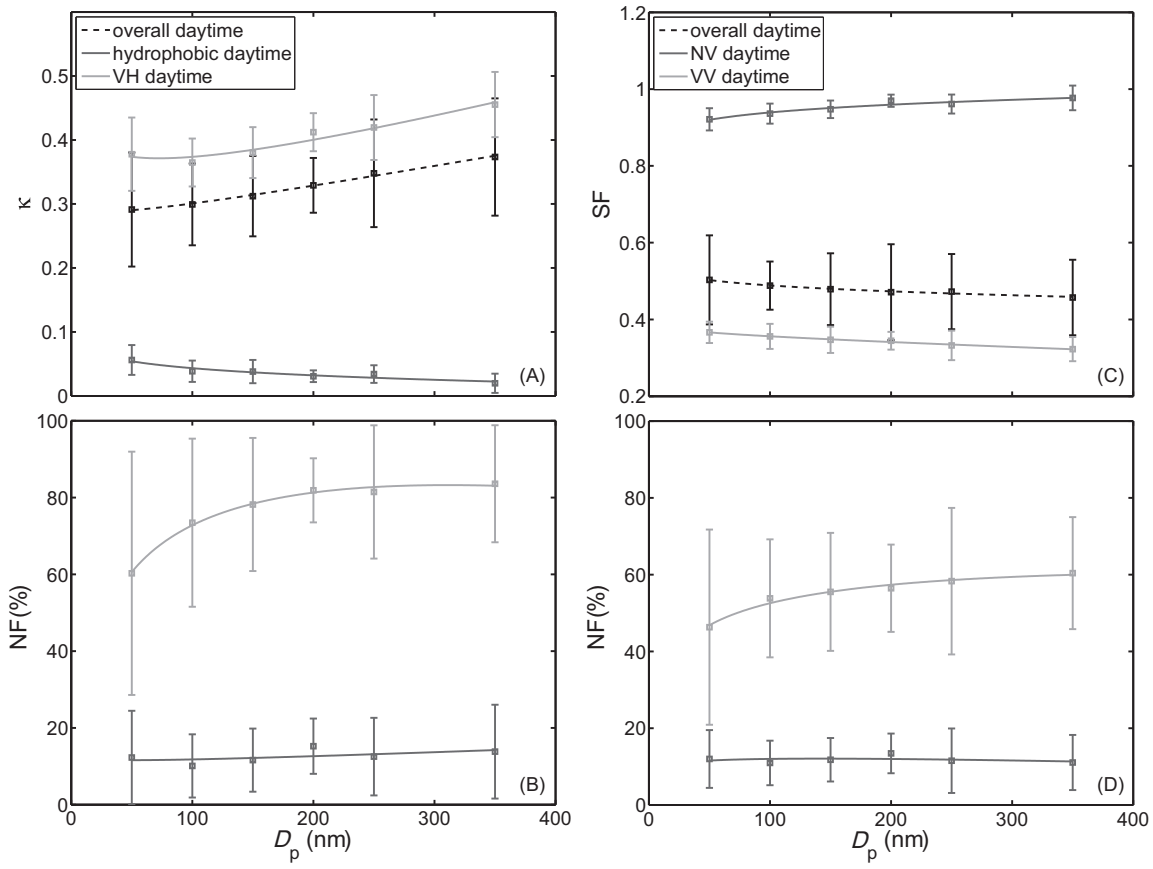

Fig. 10. Parameterization of (A) average κ for very-hydrophilic (VH) mode, hydrophobic mode and all modes, (B) average number fraction of VH mode (NF_{VH}) and hydrophobic mode (NF_{phb}), (C) average SF of very-volatile (VV) mode, non-volatile (NV) mode and all modes, (D) average number fraction of VV mode (NF_{VV}) and non-volatile mode (NF_{NV}). The lines present the results of the fittings with Eq. (10).

of two major populations. Linear relationships were found between the number fraction of hydrophobic and non-volatile particles, especially for the size larger than 100 nm, reflecting the dominance of LAC in hydrophobic and non-volatile particles. The number fraction of non-volatile particles is lower than that of hydrophobic particles in most cases, indicating that a certain fraction of hydrophobic particles are volatile.

Distinct diurnal patterns were found in the number fraction of hydrophobic and non-volatile group, with a higher level at nighttime and a lower level during the daytime. Both the number fraction of hydrophobic group and non-volatile group show peaks at around 06:00 LT and 20:00 LT, corresponding to the periods of intensive human activities. The average κ of hydrophilic particles shows a lower level in daytime than in nighttime, which is opposite to the average κ of hydrophobic group.

To investigate the influence of air mass origin and transportation on particle mixing state, our measurement data was classified according to the types of back trajectory obtained with NOAA HYSPLIT Model. It was found that the measured aerosol properties strongly depend on the residence time of the air mass over the NCP. Aerosol particles in air masses coming from north with high moving speed are less aged, therefore show a higher number fraction of hydrophobic/non-volatile group, and a more externally mixing state in terms of hygroscopicity and volatility compared with the aerosol particles in the other air mass types. Due to the active secondary particulate production over the NCP, only minor differences can be found between the measured particle properties for the rest air mass types. With abundant precursors in the NCP, regardless of the origin of air masses, aerosol particles may get aged and mixed with newly emitted particles as long as it stays in the NCP for a certain time.

Table 2
Fitting parameters for the parameterization of particle hygroscopicity and volatility.

	B	C	D
Hygroscopicity			
κ overall	−1.05e-2	3.51e-4	3.14e-1
κ VH mode	−5.23e-2	6.14e-4	5.49e-1
κ phb mode	−1.34e-2	−1.75e-5	1.07e-1
NF VH mode	2.23e-1	−6.99e-4	−2.30e-1
NFphb mode	−3.60e-2	3.01e-4	2.46e-1
Volatility			
SF overall	−1.65e-2	−1.78e-5	5.67e-1
SF VV mode	−1.14e-2	−7.28e-5	4.15e-1
SF NV mode	1.49e-2	7.61e-5	8.60e-1
NF VV mode	1.07e-1	−2.79e-4	6.15e-2
NF NV mode	−4.35e-3	3.44e-5	1.33e-1

Acknowledgment

The authors thank M. Gysel for his contribution to the TDMA inversion algorithm (TDMA*inv*), acknowledge the NOAA Air Resource Lab for their distribution of HYSPLIT, and also thank Z.Z. Deng and L. Ran from Institute of Atmospheric Physics (IAP, CAS), Y. Chen and M. Teich from Leibniz-Institute for Tropospheric Research as well as H.L. Liu from Chengdu University of Information Technology (CUIT) for the kind help. This research is supported by the projects Sino German Science center (No. GZ663)

and National Basic Research Program of China (Nos. 2013CB955801, 2013CB228503), and the National Natural Science Foundation of China (Nos. 21190052, 41305030, 41121004, 41175030).

References

Ahn, C., Torres, O., Bhartia, P.K., 2008. Comparison of ozone monitoring instrument UV aerosol products with aqua/moderate resolution imaging spectroradiometer and multiangle imaging spectroradiometer observations in 2006. J. Geophys. Res. Atmos. 113, 2008.

Birmili, W., Stratmann, F., Wiedensohler, A., Covert, D., Russell, L.M., Berg, O., 2007. Determination of differential mobility analyzer transfer functions using identical instruments in series. Aerosol Sci. Tech. 27, 215–223.

Burtscher, H., Baltensperger, U., Bukowiecki, N., Cohn, P., Huglin, C., Mohr, M., Matter, U., Nyeki, S., Schmatloch, V., Streit, N., Weingartner, E., 2001. Separation of volatile and non-volatile aerosol fractions by thermodesorption: instrumental development and applications. J. Aerosol Sci. 32, 427–442. http://dx.doi.org/10.1016/S0021-8502(00)00089-6.

Cappa, C.D., Onasch, T.B., Massoli, P., Worsnop, D.R., Bates, T.S., Cross, E.S., Davidovits, P., Hakala, J., Hayden, K.L., Jobson, B.T., Kolesar, K.R., Lack, D.A., Lerner, B.M., Li, S.M., Mellon, D., Nuaaman, I., Olfert, J.S., Petaja, T., Quinn, P.K., Song, C., Subramanian, R., Williams, E.J., Zaveri, R.A., 2012. Radiative absorption enhancements due to the mixing state of atmospheric black carbon. Science 337, 1078–1081. http://dx.doi.org/10.1126/science.1223447.

Cheng, Y.F., Berghof, M., Garland, R.M., Wiedensohler, A., Wehner, B., Muller, T., Su, H., Zhang, Y.H., Achtert, P., Nowak, A., Poschl, U., Zhu, T., Hu, M., Zeng, L.M., 2009. Influence of soot mixing state on aerosol light absorption and single scattering albedo during air mass aging at a polluted regional site in northeastern China. J. Geophys. Res. Atmos. 114. http://dx.doi.org/10.1029/2008jd010883, Artn D00g10.

Draxler, R.R., Hess, G.D., 1997. Description of the HYSPLIT_4 modeling system. NOAA Tech. Memo. ERL ARL-224, NOAA Air Resources Laboratory, Silver Spring, MD 24 pp.

Draxler, R.R., Hess, G.D., 1998. An overview of the HYSPLIT_4 modeling system of trajectories, dispersion, and deposition. Aust. Meteor. Mag. 47, 295–308.

Draxler, R.R., 1999. HYSPLIT4 user's guide. NOAA Tech. Memo. ERL ARL-230, NOAA Air Resources Laboratory, Silver Spring, MD.

Cheng, Y.F., Su, H., Rose, D., Gunthe, S.S., Berghof, M., Wehner, B., Achtert, P., Nowak, A., Takegawa, N., Kondo, Y., Shiraiwa, M., Gong, Y.G., Shao, M., Hu, M., Zhu, T., Zhang, Y.H., Carmichael, G.R., Wiedensohler, A., Andreae, M.O., Poschl, U., 2012. Size-resolved measurement of the mixing state of soot in the megacity Beijing, China: diurnal cycle, aging and parameterization. Atmos. Chem. Phys. 12, 4477–4491. http://dx.doi.org/10.5194/acp-12-4477-2012.

Ehn, N.L., Cooper, M.E., Orr, K., Shi, M., Johnson, M.K., Caprau, D., Dagle, J., Steffen, K., Johnson, K., Marazita, M.L., Merrill, D., Murray, J.C., 2007. Evaluation of fetal and maternal genetic variation in the progesterone receptor gene for contributions to preterm birth. Pediatr. Res. 62, 630–635.

Frey, A., Rose, D., Wehner, B., Muller, T., Cheng, Y.F., Wiedensohler, A., Virkkula, A., 2008. Application of the volatility-TDMA technique to determine the number size distribution and mass concentration of less volatile particles. Aerosol Sci. Tech. 42, 817–828. http://dx.doi.org/10.1080/02786820802339595.

Furutani, H., Dall'osto, M., Roberts, G.C., Prather, K.A., 2008. Assessment of the relative importance of atmospheric aging on CCN activity derived from field observations. Atmos. Environ. 42, 3130–3142. http://dx.doi.org/10.1016/j.atmosenv.2007.09.024.

Gysel, M., McFiggans, G.B., Coe, H., 2009. Inversion of tandem differential mobility analyser (TDMA) measurements. J. Aerosol Sci. 40, 134–151. http://dx.doi.org/10.1016/j.jaerosci.2008.07.013.

Harris, S.J., Maricq, M.M., 2001. Signature size distributions for diesel and gasoline engine exhaust particulate matter. J. Aerosol Sci. 32, 749–764. http://dx.doi.org/10.1016/S0021-8502(00)00111-7.

Healy, R.M., Evans, G.J., Murphy, M., Juranyi, Z., Tritscher, T., Laborde, M., Weingartner, E., Gysel, M., Poulain, L., Kamilli, K.A., Wiedensohler, A., O'Connor, I.P., McGillicuddy, E., Sodeau, J.R., Wenger, J.C., 2014. Predicting hygroscopic growth using single particle chemical composition estimates. J. Geophys. Res. Atmos. 119, 9567–9577. http://dx.doi.org/10.1002/2014jd021888.

Herich, H., Kammermann, L., Friedman, B., Gross, D.S., Weingartner, E., Lohmann, U., Spichtinger, P., Gysel, M., Baltensperger, U., Cziczo, D.J., 2009. Subarctic atmospheric aerosol composition: 2. Hygroscopic growth properties. J. Geophys. Res. Atmos. 114. http://dx.doi.org/10.1029/2008jd 011574, Artn D13204.

Hossain, A.M.M.M., Park, S., Kim, J.S., Park, K., 2012. Volatility and mixing states of ultrafine particles from biomass burning. J. Hazard. Mater. 205, 189–197. http://dx.doi.org/10.1016/j.jhazmat.2011.12.061.

Jacobson, M.Z., 2001. Strong radiative heating due to the mixing state of black carbon in atmospheric aerosols. Nature 409, 695–697. http://dx.doi.org/10.1038/35055518.

Jacobson, M.C., Hansson, H.C., Noone, K.J., Charlson, R.J., 2000. Organic atmospheric aerosols: review and state of the science. Rev. Geophys. 38, 267–294. http://dx.doi.org/10.1029/1998rg000045.

Johnson, G.R., Ristovski, Z.D., D'Anna, B., Morawska, L., 2005. Hygroscopic behavior of partially volatilized coastal marine aerosols using the volatilization and humidification tandem differential mobility analyzer technique. J. Geophys. Res. Atmos. 110. http://dx.doi.org/10.1029/2004jd005657, Artn D20203.

Kamilli, K.A., Poulain, L., Held, A., Nowak, A., Birmili, W., Wiedensohler, A., 2014. Hygroscopic properties of the Paris urban aerosol in relation to its chemical composition. Atmos. Chem. Phys. 14, 737–749. http://dx.doi.org/10.5194/acp-14-737-2014.

Kecorius, S., Zhang, S., Wang, Z., Größ, J., Ma, N., Wu, Z., Ran, L., Hu, M., Wang, P., Ulevičius, V., 2015. Nocturnal aerosol particle formation in the North China Plain. Lith. J. Phys. 55.

Kulmala, M., Dal Maso, M., Makela, J.M., Pirjola, L., Vakeva, M., Aalto, P., Miikkulainen, P., Hameri, K., O'Dowd, C.D., 2001. On the formation, growth and composition of nucleation mode particles. Tellus B 53, 479–490. http://dx.doi.org/10.1034/j.1600-0889.2001.530411.x.

Kuwata, M., Kondo, Y., 2008. Dependence of size-resolved CCN spectra on the mixing state of nonvolatile cores observed in Tokyo. J. Geophys. Res. Atmos. 113. http://dx.doi.org/10.1029/2007jd009761, Artn D19202.

Kuwata, M., Kondo, Y., Mochida, M., Takegawa, N., Kawamura, K., 2007. Dependence of CCN activity of less volatile particles on the amount of coating observed in Tokyo. J. Geophys. Res. Atmos. 112. http://dx.doi.org/10.1029/2006jd007758, Artn D11207.

Laborde, M., Crippa, M., Tritscher, T., Juranyi, Z., Decarlo, P.F., Temime-Roussel, B., Marchand, N., Eckhardt, S., Stohl, A., Baltensperger, U., Prevot, A.S.H., Weingartner, E., Gysel, M., 2013. Black carbon physical properties and mixing state in the European megacity Paris. Atmos. Chem. Phys. 13, 5831–5856. http://dx.doi.org/10.5194/acp-13-5831-2013.

Liu, W.X., Dou, H., Wei, Z.C., Chang, B., Qiu, W.X., Liu, Y., Tao, S., 2009. Emission characteristics of polycyclic aromatic hydrocarbons from combustion of different residential coals in North China. Sci. Total Environ. 407, 1436–1446. http://dx.doi.org/10.1016/j.scitotenv.2008.10.055.

Liu, P.F., Zhao, C.S., Gobel, T., Hallbauer, E., Nowak, A., Ran, L., Xu, W.Y., Deng, Z.Z., Ma, N., Mildenberger, K., Henning, S., Stratmann, F., Wiedensohler, A., 2011. Hygroscopic properties of aerosol particles at high relative humidity and their diurnal variations in the North China Plain. Atmos. Chem. Phys. 11, 3479–3494. http://dx.doi.org/10.5194/acp-11-3479-2011.

Liu, K.K., Zhang, C.L., Cheng, Y., Liu, C.T., Zhang, H.X., Zhang, G., Sun, X., Mu, Y.J., 2015. Serious BTEX pollution in rural area of the North China Plain during winter season. J. Environ. Sci. China 30, 186–190. http://dx.doi.org/10.1016/j.jes.2014.05.056.

Livingston, J.M., Redemann, J., Russell, P.B., Torres, O., Veihelmann, B., Veefkind, P., Braak, R., Smirnov, A., Remer, L., Bergstrom, R.W., Coddington, O., Schmidt, K.S., Pilewskie, P., Johnson, R., Zhang, Q., 2009. Comparison of aerosol optical depths from the ozone monitoring instrument (OMI) on aura with results from airborne sunphotometry, other space and ground measurements during MILAGRO/INTEX-B. Atmos. Chem. Phys. 9, 6743–6765.

Londahl, J., Swietlicki, E., Lindgren, E., Loft, S., 2010. Aerosol exposure versus aerosol cooling of climate: what is the optimal emission reduction strategy for human health? Atmos. Chem. Phys. 10, 9441–9449. http://dx.doi.org/10.5194/acp-10-9441-2010.

Ma, N., Zhao, C.S., Nowak, A., Müller, T., Pfeifer, S., Cheng, Y.F., Deng, Z.Z., Liu, P.F., Xu, W.Y., Ran, L., Yan, P., Göbel, T., Hallbauer, E., Mildenberger, K., Henning, S., Yu, J., Chen, L.L., Zhou, X.J., Stratmann, F., Wiedensohler, A., 2011. Aerosol optical properties in the North China Plain during HaChi campaign: an in-situ optical closure study. Atmos. Chem. Phys. 11, 5959–5973. http://dx.doi.org/10.5194/acp-11-5959-2011.

Ma, N., Zhao, C.S., Müller, T., Cheng, Y.F., Liu, P.F., Deng, Z.Z., Xu, W.Y., Ran, L., Nekat, B., van Pinxteren, D., Gnauk, T., Müller, K., Herrmann, H., Yan, P., Zhou, X.J., Wiedensohler, A., 2012. A new method to determine the mixing state of light absorbing carbonaceous using the measured aerosol optical properties and number size distributions. Atmos. Chem. Phys. 12, 2381–2397. http://dx.doi.org/10.5194/acp-12-2381-2012.

Massling, A., Wiedensohler, A., Busch, B., Neususs, C., Quinn, P., Bates, T., Covert, D., 2003. Hygroscopic properties of different aerosol types over the Atlantic and Indian Oceans. Atmos. Chem. Phys. 3, 1377–1397. http://dx.doi.org/10.5194/acp-3-1377-2003.

Massling, A., Leinert, S., Wiedensohler, A., Covert, D., 2007. Hygroscopic growth of sub-micrometer and one-micrometer aerosol particles measured during ACE-Asia. Atmos. Chem. Phys. 7, 3249–3259.

Massling, A., Stock, M., Wehner, B., Wu, Z.J., Hu, M., Bruggemann, E., Gnauk, T., Herrmann, H., Wiedensohler, A., 2009. Size segregated water uptake of the urban submicrometer aerosol in Beijing. Atmos. Environ. 43, 1578–1589. http://dx.doi.org/10.1016/j.atmosenv.2008.06.003.

Meng, Z.Y., Xu, X.B., Yan, P., Ding, G.A., Tang, J., Lin, W.L., Xu, X.D., Wang, S.F., 2009. Characteristics of trace gaseous pollutants at a regional background station in Northern China. Atmos. Chem. Phys. 9, 927–936.

Moffet, R.C., Prather, K.A., 2009. In-situ measurements of the mixing state and optical properties of soot with implications for radiative forcing estimates. Proc. Natl. Acad. Sci. U. S. A. 106, 11872–11877. http://dx.doi.org/10.1073/pnas.0900040106.

Nordmann, S., Cheng, Y.F., Carmichael, G.R., Yu, M., van der Gon, H.A.C.D., Zhang, Q., Saide, P.E., Poschl, U., Su, H., Birmili, W., Wiedensohler, A., 2014. Atmospheric black carbon and warming effects influenced by the source and absorption enhancement in central Europe. Atmos. Chem. Phys. 14, 12683–12699. http://dx.doi.org/10.5194/acp-14-12683-2014.

Oshima, N., Koike, M., Zhang, Y., Kondo, Y., 2009. Aging of black carbon in outflow from anthropogenic sources using a mixing state resolved model: 2. Aerosol optical properties and cloud condensation nuclei activities. J. Geophys. Res. Atmos. 114. http://dx.doi.org/10.1029/2008jd011681, Artn D18202.

Petters, M.D., Kreidenweis, S.M., 2007. A single parameter representation of hygroscopic growth and cloud condensation nucleus activity. Atmos. Chem. Phys. 7, 1961–1971.

Petters, M.D., Prenni, A.J., Kreidenweis, S.M., DeMott, P.J., Matsunaga, A., Lim, Y.B., Ziemann, P.J., 2006. Chemical aging and the hydrophobic-to-hydrophilic conversion of carbonaceous aerosol. Geophys. Res. Lett. 33. http://dx.doi.org/10.1029/2006gl027249, Artn L24806.

Petzold, A., Schonlinner, M., 2004. Multi-angle absorption photometry – a new method for the measurement of aerosol light absorption and atmospheric black carbon. J. Aerosol Sci. 35, 421–441. http://dx.doi.org/10.1016/j.jaerosci.2003.09.005.

Philippin, S., Wiedensohler, A., Stratmann, F., 2004. Measurements of non-volatile fractions of pollution aerosols with an eight-tube volatility tandem differential mobility analyzer (VTDMA-8). J. Aerosol Sci. 35, 185–203. http://dx.doi.org/10.1016/j.jaerosci.2003.07.004.

Reddington, C.L., McMeeking, G., Mann, G.W., Coe, H., Frontoso, M.G., Liu, D., Flynn, M., Spracklen, D.V., Carslaw, K.S., 2013. The mass and number size distributions of black carbon aerosol over Europe. Atmos. Chem. Phys. 13, 4917–4939. http://dx.doi.org/10.5194/acp-13-4917-2013.

Riemer, N., West, M., Zaveri, R.A., Easter, R.C., 2009. Simulating the evolution of soot mixing state with a particle-resolved aerosol model. J. Geophys. Res. Atmos. 114. http://dx.doi.org/10.1029/2008jd 011073, Artn D09202.

Riemer, N., West, M., Zaveri, R., Easter, R., 2010. Estimating black carbon aging timescales with a particle-resolved aerosol model. J. Aerosol Sci. 41, 143–158. http://dx.doi.org/10.1016/j.jaerosci.2009.08.009.

Rissler, J., Vestin, A., Swietlicki, E., Fisch, G., Zhou, J., Artaxo, P., Andreae, M.O., 2006. Size distribution and hygroscopic properties of aerosol particles from dry-season biomass burning in Amazonia. Atmos. Chem. Phys. 6, 471–491.

Rose, D., Wehner, B., Ketzel, M., Engler, C., Voigtlander, J., Tuch, T., Wiedensohler, A., 2006. Atmospheric number size distributions of soot particles and estimation of emission factors. Atmos. Chem. Phys. 6, 1021–1031.

Rose, D., Gunthe, S.S., Su, H., Garland, R.M., Yang, H., Berghof, M., Cheng, Y.F., Wehner, B., Achtert, P., Nowak, A., Wiedensohler, A., Takegawa, N., Kondo, Y., Hu, M., Zhang, Y., Andreae, M.O., Poschl, U., 2011. Cloud condensation nuclei in polluted air and biomass burning smoke near the mega-city Guangzhou, China -Part 2: size-resolved aerosol chemical composition, diurnal cycles, and externally mixed weakly CCN-active soot particles. Atmos. Chem. Phys. 11, 2817–2836. http://dx.doi.org/10.5194/acp-11-2817-2011.

Sakurai, H., Tobias, H.J., Park, K., Zarling, D., Docherty, K.S., Kittelson, D.B., Mcmurry, P.H., Ziemann, P.J., 2003. On-line measurements of diesel nanoparticle composition and volatility. Atmos. Environ. 37, 1199–1210.

Schnelle-Kreis, J., Kupper, U., Sklorz, M., Cyrys, J., Briede, J.J., Peters, A., Zimmermann, R., 2009. Daily measurement of organic compounds in ambient particulate matter in Augsburg, Germany: new aspects on aerosol sources and aerosol related health effects. Biomarkers 14, 39–44. http://dx.doi.org/10.1080/13547500902965997.

Shen, J.L., Liu, X.J., Zhang, Y., Fangmeier, A., Goulding, K., Zhang, F.S., 2011. Atmospheric ammonia and particulate ammonium from agricultural sources in the North China Plain. Atmos. Environ. 45, 5033–5041. http://dx.doi.org/10.1016/j.atmosenv.2011.02.031.

Swietlicki, E., Hansson, H.C., Hameri, K., Svenningsson, B., Massling, A., McFiggans, G., McMurry, P.H., Petaja, T., Tunved, P., Gysel, M., Topping, D., Weingartner, E., Baltensperger, U., Rissler, J., Wiedensohler, A., Kulmala, M., 2008. Hygroscopic properties of submicrometer atmospheric aerosol particles measured with H-TDMA instruments in various environments – a review. Tellus B 60, 432–469. http://dx.doi.org/10.1111/j.1600-0889.2008.00350.x.

Tan, H.B., Yin, Y., Gu, X.S., Li, F., Chan, P.W., Xu, H.B., Deng, X.J., Wan, Q.L., 2013. An observational study of the hygroscopic properties of aerosols over the Pearl River Delta region. Atmos. Environ. 77, 817–826. http://dx.doi.org/10.1016/j.atmosenv.2013.05.049.

Tao, M.H., Chen, L.F., Su, L., Tao, J.H., 2012. Satellite observation of regional haze pollution over the North China Plain. J. Geophys. Res. Atmos. 117. http://dx.doi.org/10.1029/2012jd017915, Artn D12203.

Tiitta, P., Miettinen, P., Vaattovaara, P., Joutsensaari, J., Petaja, T., Virtanen, A., Raatikainen, T., Aalto, P., Portin, H., Romakkaniemi, S., Kokkola, H., Lehtinen, K.E.J., Kulmala, M., Laaksonen, A., 2010. Roadside aerosol study using hygroscopic, organic and volatility TDMAs: characterization and mixing state. Atmos. Environ. 44, 976–986. http://dx.doi.org/10.1016/j.atmosenv.2009.06.021.

Tuch, T.M., Haudek, A., Muller, T., Nowak, A., Wex, H., Wiedensohler, A., 2009. Design and performance of an automatic regenerating adsorption aerosol dryer for continuous operation at monitoring sites. Atmos. Meas. Tech. 2, 417–422.

Wehner, B., Birmili, W., Ditas, F., Wu, Z., Hu, M., Liu, X., Mao, J., Sugimoto, N., Wiedensohler, A., 2008. Relationships between submicrometer particulate air pollution and air mass history in Beijing, China, 2004–2006. Atmos. Chem. Phys. 8, 6155–6168.

Wehner, B., Berghof, M., Cheng, Y.F., Achtert, P., Birmili, W., Nowak, A., Wiedensohler, A., Garland, R.M., Poschl, U., Hu, M., Zhu, T., 2009. Mixing state of non-volatile aerosol particle fractions and comparison with light absorption in the polluted Beijing region. J. Geophys. Res. Atmos. 114. http://dx.doi.org/10.1029/2008jd010923, Artn D00g17.

Wiedensohler, A., 1988. An approximation of the bipolar charge-distribution for particles in the sub-micron size range. J. Aerosol Sci. 19, 387–389. http://dx.doi.org/10.1016/0021-8502(88)90278-9.

Wiedensohler, A., Cheng, Y.F., Nowak, A., Wehner, B., Achtert, P., Berghof, M., Birmili, W., Wu, Z.J., Hu, M., Zhu, T., Takegawa, N., Kita, K., Kondo, Y., Lou, S.R., Hofzumahaus, A., Holland, F., Wahner, A., Gunthe, S.S., Rose, D., Su, H., Poschl, U., 2009. Rapid aerosol particle growth and increase of cloud condensation nucleus activity by secondary aerosol formation and condensation: a case study for regional air pollution in northeastern China. J. Geophys. Res. Atmos. 114. http://dx.doi.org/10.1029/2008jd010884, Artn D00g08.

Wiedensohler, A., Birmili, W., Nowak, A., Sonntag, A., Weinhold, K., Merkel, M., Wehner, B., Tuch, T., Pfeifer, S., Fiebig, M., Fjaraa, A.M., Asmi, E., Sellegri, K., Depuy, R., Venzac, H., Villani, P., Laj, P., Aalto, P., Ogren, J.A., Swietlicki, E., Williams, P., Roldin, P., Quincey, P., Huglin, C., Fierz-Schmidhauser, R., Gysel, M., Weingartner, E., Riccobono, F., Santos, S., Gruning, C., Faloon, K., Beddows, D., Harrison, R.M., Monahan, C., Jennings, S.G., O'Dowd, C.D., Marinoni, A., Horn, H.G., Keck, L., Jiang, J., Scheckman, J., McMurry, P.H., Deng, Z., Zhao, C.S., Moerman, M., Henzing, B., de Leeuw, G., Loschau, G., Bastian, S., 2012. Mobility particle size spectrometers: harmonization of technical standards and data structure to facilitate high quality long-term observations of atmospheric particle number size distributions. Atmos. Meas. Tech. 5, 657–685. http://dx.doi.org/10.5194/amt-5-657-2012.

Wiedensohler, A., Birmili, W., Putaud, J.-P., Ogren, J., 2013. Recommendations for aerosol sampling. Aerosol Science. John Wiley & Sons, Ltd, pp. 45–59.

Wiedensohler, A., Orsini, D., Covert, D.S., Coffmann, D., Cantrell, W., Havlicek, M., Brechtel, F.J., Russell, L.M., Weber, R.J., Gras, J., 2007. Intercomparison study of the size-dependent counting efficiency of 26 condensation particle counters. Aerosol Sci. Tech. 27, 224–242.

Wu, Z., Birmili, W., Poulain, L., Poulain, L., Merkel, M., Fahlbusch, B., van Pinxteren, D., Herrmann, H., Wiedensohler, A., 2013. Particle hygroscopicity during atmospheric new particle formation events: implications for the chemical species contributing to particle growth. Atmos. Chem. Phys. 13, 6637–6646. http://dx.doi.org/10.5194/acp-13-6637-2013.

Wu, Z.J., Poulain, L., Henning, S., Dieckmann, K., Birmili, W., Merkel, M., van Pinxteren, D., Spindler, G., Muller, K., Stratmann, F., Herrmann, H., Wiedensohler, A., 2013. Relating particle hygroscopicity and CCN activity to chemical composition during the HCCT-2010 field campaign. Atmos. Chem. Phys. 13, 7983–7996. http://dx.doi.org/10.5194/acp-13-7983-2013.

Xu, W.Y., Zhao, C.S., Ran, L., Deng, Z.Z., Liu, P.F., Ma, N., Lin, W.L., Xu, X.B., Yan, P., He, X., Yu, J., Liang, W.D., Chen, L.L., 2011. Characteristics of pollutants and their correlation to meteorological conditions at a suburban site in the North China Plain. Atmos. Chem. Phys. 11, 4353–4369. http://dx.doi.org/10.5194/acp-11-4353-2011.

Yang, L.X., Gao, X.M., Wang, X.F., Nie, W., Wang, J., Gao, R., Xu, P.J., Shou, Y.P., Zhang, Q.Z., Wang, W.X., 2014. Impacts of firecracker burning on aerosol chemical characteristics and human health risk levels during the Chinese New Year celebration in Jinan, China. Sci. Total Environ. 476, 57–64. http://dx.doi.org/10.1016/j.scitotenv.2013.12.110.

Yue, D.L., Hu, M., Zhang, R.Y., Wu, Z.J., Su, H., Wang, Z.B., Peng, J.F., He, L.Y., Huang, X.F., Gong, Y.G., Wiedensohler, A., 2011. Potential contribution of new particle formation to cloud condensation nuclei in Beijing. Atmos. Environ. 45, 6070–6077. http://dx.doi.org/10.1016/j.atmosenv.2011.07.037.

Zaveri, R.A., Barnard, J.C., Easter, R.C., Riemer, N., West, M., 2010. Particle-resolved simulation of aerosol size, composition, mixing state, and the associated optical and cloud condensation nuclei activation properties in an evolving urban plume. J. Geophys. Res. Atmos. 115. http://dx.doi.org/10.1029/2009jd 013616, Artn D17210.

Zelenyuk, A., Imre, D., Earle, M., Easter, R., Korolev, A., Leaitch, R., Liu, P., Macdonald, A.M., Ovchinnikov, M., Strapp, W., 2010. Situ characterization of cloud condensation nuclei, interstitial, and background particles using the single particle mass spectrometer, SPLAT II. Anal. Chem. 82, 7943–7951. http://dx.doi.org/10.1021/Ac1013892.

Zhang, R.Y., Khalizov, A.F., Pagels, J., Zhang, D., Xue, H.X., McMurry, P.H., 2008. Variability in morphology, hygroscopicity, and optical properties of soot aerosols during atmospheric processing. Proc. Natl. Acad. Sci. U. S. A. 105, 10291–10296. http://dx.doi.org/10.1073/pnas.0804860105.

Zhang, J.C., Wang, L., Chen, J.M., Feng, S.M., Shen, J.D., Jiao, L., 2011. Hygroscopicity of ambient submicron particles in urban Hangzhou, China. Front. Environ. Sci. En. 5, 342–347. http://dx.doi.org/10.1007/s11783-011-0358-7.

Zhang, Y.M., Zhang, X.Y., Sun, J.Y., Hu, G.Y., Shen, X.J., Wang, Y.Q., Wang, T.T., Wang, D.Z., Zhao, Y., 2014. Chemical composition and mass size distribution of PM1 at an elevated site in central east China. Atmos. Chem. Phys. 14, 12237–12249. http://dx.doi.org/10.5194/acp-14-12237-2014.

Zhuang, B.L., Li, S., Wang, T.J., Deng, J.J., Xie, M., Yin, C.Q., Zhu, J.L., 2013. Direct radiative forcing and climate effects of anthropogenic aerosols with different mixing states over China. Atmos. Environ. 79, 349–361. http://dx.doi.org/10.1016/j.atmosenv.2013.07.004.

Zong, Z., Chen, Y.J., Tian, C.G., Fang, Y., Wang, X.P., Huang, G.P., Zhang, F., Li, J., Zhang, G., 2015. Radiocarbon-based impact assessment of open biomass burning on regional carbonaceous aerosols in North China. Sci. Total Environ. 518, 1–7. http://dx.doi.org/10.1016/j.scitotenv.2015.01.113.